SPE 121054

Temperature Modeling and Analysis of Wells with Advanced Completion

K.M. Muradov and D.R. Davies, SPE, Heriot-Watt University, Edinburgh, U.K.

This paper was prepared for presentation at the 2009 SPE EUROPEC/EAGE Annual Conference and Exhibition held in Amsterdam, The Netherlands, 8–11 June 2009.

Abstract

Advanced completions using technologies such as Inflow Control Devices or Interval Control Valves are successfully optimising oil and gas production. They are often accompanied by the installation of Distributed Temperature Sensors and Permanent Downhole Gauges, providing continuous, real-time monitoring of the downhole pressure and temperature. Interpretation of such data to locate influxes and to track zonal inflow performance is an important step towards a comprehensive well and field control strategy.

Interpretation of these downhole measurements requires accurate modelling of the well's pressure and temperature. Modelling of the pressures associated with the production of wells with advanced completion has been available for sometime. However, the workflow required for temperature modelling is not yet complete. This paper discusses using available theoretical models and software tools to model the temperature distribution in wells with advanced completion. The strengths and weaknesses of the various approaches for data interpretation will be discussed.

Several methods for the quantitative interpretation of downhole temperature measurements are proposed. The application of both currently available and novel theoretical models will be discussed. The workflow will be shown to be capable of providing both zonal flow rates and phase compositions.

The interpretation and analysis techniques presented here form the basis of a well and/or field monitoring and production control workflow.

1.0 Introduction

The installation of advanced well completions is increasing in popularity[1,2] worldwide. One of the main priorities of these technologies is the creation and improvement of hardware for monitoring, managing and controlling the well inflow at the level of an individual zone. The control capabilities of these devices can be subdivided into active {Interval Control Valves (ICVs)} and passive {Inflow Control Devices (ICDs)} while autonomous ICDs combine features from both devices.

They are able to solve a wide range of fluid production problems[3,4]. ICDs are installed to ensure a uniform production or injection profile along the complete completion length of the well, thus delaying breakthrough, improving clean-up, optimizing injection or steam-assisted gravity drainage, etc. ICVs are being used for recovery optimization in complex reservoirs and/or wells where the completion is required to dynamically respond to changing and uncertain production behaviour[5]. Efficient inflow (or outflow) control rests on the availability of an advanced monitoring system which provides real-time values of the phase flow distribution in the well.

Modern downhole monitoring devices, installed as part of the advanced completion, provide sufficient information that they, along with the flow control hardware, form the basis of the intelligent field. Advanced monitoring technologies, such as optical fibre based Distributed Temperature or Pressure Sensors (DTS or DPS), Permanently installed Downhole Gauges (PDG), multiphase flow meters, etc., produce large amounts of downhole data in real-time[6,7]. Traditional analytical approaches have proved to be insufficient to retrieve useful information from the vast quantities of downhole data provided by the increasing employment of temperature and pressure measurement sensors. The realisation that temperature behaviour is a complex process that has had less research attention than its pressure counterpart resulted in the initiation of research in this area of petroleum data processing and analysis. A significant part of this effort has been directed towards the analysis of temperature data to evaluate flow rates and phase distributions at specific points along the completion's length

In this paper we will discuss the success of several available analytical and simulation tools to accurately model steady-state, temperature and pressure profiles in wells. The ability to estimate phase rates in wells completed with ICDs and/or ICVs will be discussed. We will also present several novel analytical solutions on reservoir temperature distribution calculation. Finally a group of calculation methods to estimate inflow and permeability distributions and flow rate profiles will be presented.

2.0 Modelling of Temperature and Pressure Profiles in Wells

Pressure modelling in pipes has been extensively studied for many years[8], but is still being improved. Our proposed calculation procedure will incorporate well proven, previously published, pressure correlations (Beggs and Brill, Hagedorn and Brown). Temperature modelling has been approached by using either a general theoretical model[9] or with commercial simulators.

Our objective is to use accurate temperature and pressure models to be able to quantify zonal, multi-phase flow rates. This objective will form the basis of our test protocol. The test model for this comparative test consists of one vertical segment of 300 ft length with uniform inflow into the annulus from the formation (Figure 1). Errors in the predicted flow rates are calculated based on the assumption that there is a permanent downhole gauge installed at the top of the segment with a measurement error of ± 0.2 °F. The applicability of the various temperature prediction methods for flow rate monitoring will be illustrated by calculating the difference in the rate prediction, based on the temperature deviation from the "real" data, using different analysis methods.

The remainder of section will describe the theoretical models, providing us with a clear view of which effects are essential and which ones can be omitted. The study has been limited to isothermal reservoir performance (i.e. sand face temperature equals the geothermal value) in this comparison study.

2.1 Available Analytical Solutions

The accurate temperature prediction model[9] used here accounts for the transfer processes in wells with advanced completion operating in steady state flow. The model's general solution for the case of simultaneous annular and tubing multiphase flows can be summarised as a system of two equations:

$$\begin{cases} \dfrac{dT_a}{dx} = \dfrac{2\pi R_{ci}(1-\delta)U_{awb}(T_{wb}-T_a) - 2\pi R_{ti}U_{at}(T_a-T_t) + \left(w' C_p (T_I - T_a)\right)_I + (w)_a g\sin\theta + \left[(wC_pK_{JT})_a + h_{lat,jj'} w_{aj'}\left(\dfrac{\rho_{aj}}{\rho_{aj'}}\dfrac{dR_s}{dp}\bigg|_T\right)\right]\dfrac{dp_a}{dx}}{(wC_p)_a} \\ \dfrac{dT_t}{dx} = \dfrac{2\pi R_{ti}U_{at}(T_a-T_t) + (w)_t g\sin\theta + \left[(wC_pK_{JT})_t + h_{lat,jj'} w_{tj'}\left(\dfrac{\rho_{tj}}{\rho_{tj'}}\dfrac{dR_s}{dp}\bigg|_T\right)\right]\dfrac{dp_t}{dx}}{(wC_p)_t} \end{cases} \quad (1a,b)$$

where U is the heat transfer coefficient, K_{JT} – the Joule-Thomson coefficient, w - the mass flow rate, subscripts a, t and f stand for *annular*, *tubing* and *formation* respectively; and subscripts by the brackets mean summation of phase properties in the brackets over the subscripted volume (see notations). The equations describing the heat transfer coefficients are already available[10,11]. The resulting temperature profiles from the numerical[9] solution of equations (1a,b) are shown in Figure 2. These profiles form the base case against which we will match our simulation results (hence the top temperature values represent gauge measurements).

2.2 Simulators

The following simulators have been tested on their ability for accurate flow rate prediction based on the temperature data as described above:

1. Several steady-state, well flow simulators.
2. A reservoir simulator capable of simulating both thermal effects and a segmented well.
3. A dynamic well flow simulator.

2.2.1 Steady-State Well Flow Simulators

All the evaluated steady-state, well flow simulators perform in a similar manner. They produced similar results (they use similar algorithms for temperature modelling; hence the resulting mismatch with our base case was also similar).

These simulators can emulate continuous inflow into the annulus by placing multiple sources along the annular flow path. However, the important process of heat exchange between the tubing and the annulus is not captured. We evaluated reducing this effect by defining the heat transfer coefficient of the pipe representing tubing as the value of the annular heat transfer coefficient in the middle of the interval. The temperature gradient outside the tubing was assumed to be 50% of the geothermal value (the best initial guess for the annular temperature emulation, see Figure 2). The resulting annulus temperature is lower than the reference result (Figure 3). The only way to raise it is by increasing the inflow rate sufficiently that the pressure drop causes extra Joule-Thomson heating. Table 1 shows that the resulting, predicted rate value is far from the real one.

This illustrates how strongly tubing-annulus flow acts as an effective heat exchanger. Annular temperature values are significantly lower than in the base case since the fluid is not receiving additional heat from the tubing. The tubing temperature profile is also different. Simulation of tubing-annulus heat exchange which varies with depth is difficult. It is theoretically possible to manually calculate the missing heat exchange effect which would then be introduced iteratively into the program.

However, this task is laborious, time consuming and is not an acceptable solution for real-time rate estimation problems.

2.2.2 Combined Thermal Reservoir and segmented Well Simulator

We were given access to a reservoir simulator that was able to simulate well segments and thermal effects. Its capabilities allow modelling of thermal coupling between the tubing and annulus. Unfortunately, the heat transfer coefficients for every well segment need to be defined manually. This is not a simple task, since their numerical values vary depending on the fluid velocity[10,11], a factor which increases significantly over the well's length. It proved possible to obtain accurate results with this simulator by first (manually) calculating and then (manually) introducing the heat-transfer coefficient values for every segment into the program (Figure 4 and Table 1). However, as for the well simulator, this is a laborious, time-consuming process. The discrepancy between the calculated and the base case temperature profiles (Figure 4) are thought to be due to errors caused by the well segmentation and the Joule-Thomson effect calculations.

In conclusion, the combined Thermal Reservoir and segmented Well Simulator has limited use for our purposes since each change in flow rate has to be reflected by manual changes in the heat transfer coefficients for each segment.

2.2.3 Dynamic Well Flow Simulator

The dynamic well flow simulator has sufficient flexibility for modelling our problem. It allows building a model capable of correct flow rate performance prediction for complicated (advanced) completion designs. Continuous inflow into the annulus is emulated by multiple sources along its length. The thermal interaction present in intelligent wells between the tubing and annulus is simulated by using annular thermal coupling. The required heat transfer coefficients are calculated in-situ. Hence the major thermal effects are covered.

Figure 2 shows that our analytical model and this simulator provide very similar temperature profiles. Examples of such similarity for more complex cases (multi-zone wells with multiphase flow) can also be found in published literature[16].

2.3 Conclusions from the Evaluation of Available Temperature Modelling Tools

We have shown that the steady-state, well flow simulators and a thermal reservoir and well segment simulator are not suitable for use as flow rate estimation tools based on temperature data, either due to technical reasons (time-consuming and laborious) or due to the omission of the required physics. The dynamic well flow simulator provides the correct temperature profiles for complex wells. However, the calculation of the inverse problem (the estimation of flow rates on the basis of temperature data) is also a complex process in this simulator.

Hence the dynamic well flow simulator can be employed, for example, as a reference software to provide the base case model results in order to evaluate response sensitivity of a system or for other purposes. The analytical temperature model has sufficient flexibility to be used as a reference as well as a basic tool for real-time data analysis. Table 2 summarises these conclusions.

3.0 Calculation of Sandface Temperature

Calculation of the temperature and pressure profiles in a well is intimately connected to the value of the sandface temperature and pressure, both of which are a reflection of the reservoir performance. Transient, thermal interaction between the well and the ambient layers when the reservoir fluids are stationary has been previously described[12]. A mathematical model for the temperature calculations in an isolated reservoir around a horizontal well in steady-state liquid flow has also been published[13]. It was later extended to model both a layer that thermally interacts with adjacent layers in the case of inflow into a horizontal well and for an isolated producing layer around a vertical well[9]. The following will generalise these models by deriving the necessary equations for the sandface temperature calculations for a flowing well in which the reservoir thermally interacts with the adjacent layers.

Our description starts when a sufficient time has passed since production started that a limited volume around the well can be described as having both steady-state fluid and heat flows (Figure 5, Figure 6). We will also assume that this volume of rock is incompressible, that the reservoir layer is horizontal and isotropic and that there is no mass transfer between phases. The equation for this region is[9]:

$$\sum_j \vec{v}_j \left[\rho_j C_{p,j} \vec{\nabla} T_f + (1-\beta_j T_f)\vec{\nabla} p_j\right] - \vec{\nabla}(\overline{\overline{K_f}}\vec{\nabla} T_f) + 2U_{adj}(T_f - T_{f,geothermal})/h = 0 \qquad (2)$$

where subscript *j* corresponds to flowing phases, subscript *adj* stands for *adjacent* (layers), $\overline{\overline{K_f}}$ is the formation thermal conductivity tensor and *h* the reservoir thickness. The terms in equation (2) correspond to (in order): convection, Joule-Thomson effect, conduction, and thermal interaction with adjacent layers.

The value of the transient heat transfer coefficient of layers thermal interaction U_{adj} can be approximated as[14]:

$$U_{adj} = 2\sqrt{\frac{K_{f,adj}\rho_{f,adj}C_{pf,adj}}{\pi t}} \qquad (3)$$

where *t* is the production time.

3.1 Sandface Temperature for Horizontal Well – Asymptotic Solution for Liquid Flow

Equation (2) contains the fluid density. The numerical value of the density will vary significantly as a function of pressure for gases (A-7) while it is approximately constant for liquids. Thus different analytical solutions are required for gas and liquid flow. We have therefore subdivided our problem into two, one for gases and one for liquids that will be combined later.

The full solution for the case of liquid flow is already available[9]. Since normally

$$\frac{4K_f}{(wC)_I^2}\left(\frac{\beta q^2 \mu}{k}\right)_I << 1 \tag{4}$$

and

$$R_{wb}\Big/R_e << 1 \tag{5}$$

the asymptotic solution for the sandface temperature is:

$$T_{wb} \approx T_e - \left(K'_{JT,l}(P_e - P_{wb})\frac{(1-e^{-2C_{adj}})}{2C_{adj}} - \alpha(T_a - T_e)\right)\Big/(1+\alpha) \tag{6}$$

where $K'_{JT,l}$ corresponds to the appropriate average value of the liquids' Joule-Thomson coefficient:

$$K'_{JT,l} = -\frac{k_o}{\mu_o q_o}\frac{1}{(wC_p)_I}\left(\frac{q^2\mu}{k}\right)_I\left[1 - T_e\left(\frac{\beta q^2\mu}{k}\right)_I\Big/\left(\frac{q^2\mu}{k}\right)_I\right] \tag{7}$$

C_{adj} represents the correction factor due to the heat thermal interaction with adjacent layers:

$$C_{adj} = \frac{Y}{8\left|(wC_p)_I\right|hL}\left[\left(\frac{\beta q^2\mu}{k}\right)_I + 8hL^2U_{adj}\right] \approx \frac{YLU_{adj}}{\left|(wC_p)_I\right|} = \frac{A_{res,I}U_{adj}}{\left|(wC_p)_I\right|} \tag{8}$$

where $A_{res,I}$ is the reservoir area contributing to the inflow being considered.

α in equation (6) is a correction term corresponding to the wellbore/near-wellbore zone thermal equilibrium:

$$\alpha = \frac{2\pi LU_{awb}R_{ci}}{\left|(wC_p)_I\right|} \tag{9}$$

Heat and fluid flow near any well can be described as radial. Hence the correction term (α) is a general description which accounts for the thermal equilibrium. The general equation can now be solved by assuming zero reservoir thermal conductivity; providing that this correction term is added to the final solution.

The solution {equation (6)} demonstrates that the sandface temperature is the reservoir boundary temperature adjusted by Joule-Thomson heating in the drainage area after correction for the thermal interaction with the adjacent layers and for the wellbore/near-wellbore zone thermal equilibrium.

The modified Joule-Thomson coefficient {equation (7)} reflects a unique averaging of flowing liquid properties.

3.2 General Asymptotic View and Solution for Other Cases

We assume that the correction factor C_{adj} {Equation (8)}, that represents the contribution of the thermal interaction of the reservoir with adjacent layers, has a low value for flowing reservoir:

$$C_{adj} << 1 \tag{10}$$

If condition (10) is not valid, i.e. thermal interaction between adjacent layers is much higher than the Joule-Thomson temperature change inside the reservoir, then the inflow temperature almost equals the geothermal value and the above thermal calculations can be avoided. Assumption (10) allows further simplification of the asymptotic solution to:

$$T_{wb} \approx T_e - \left(K'_{JT}(1 - C_{adj}\Big/\gamma)(P_e - P_{wb}) - \alpha(T_a - T_e)\right)\Big/(1+\alpha) \tag{11}$$

This is the general solution we will be using to evaluate temperature change in the reservoir. It describes how the reservoir temperature is reduced by the Joule-Thomson effect. This is itself reduced by thermal interaction with adjacent layers during the flow (first term in the numerator) and also by the wellbore/near-wellbore zone thermal equilibrium (second term in the numerator and the denominator).

An example temperature distribution for liquids around a vertical well is presented in Figure 7. This figure illustrates that a near-wellbore, thermal equilibrium zone (where temperature deviates from the Joule-Thomson trend) is thin. It may be insufficient to affect the temperature of the fluid flowing through it. We further suggest using equation (11) for the sandface temperature calculation and that the fluid inflow temperature is calculated without the equilibrium correction {zero α in equation (11)}. Note that the equilibrium zone thickness depends on the flow rate value: for very low flow rates (which we do not consider in this paper) the zone can be sufficiently thick – this is a matter of a separate research.

A case-specific, modified Joule-Thomson coefficient is derived by solving the general equation (2) directly without the formation conductivity and adjacent layer interaction terms. The required equations of state and pressure distribution terms were used. The correction for the thermal interaction between layers occurs when equation (2) is solved with the appropriate term present. The equilibrium correction is commonly applied to the resulting solution. Appendix A presents mathematical descriptions for both liquid and gas flow around both horizontal and vertical wells. Table 3 summarises the resulting coefficients.

3.3 Inclined Wells and Gas-Liquid Flow

The above cases consider only vertical or horizontal wells. Wells with other trajectories will cause the same temperature drop in the reservoir (the effect of well inclination is already accounted for in the pressure drop) apart from the effect of the well-reservoir heat transfer. This latter is a function of the well area exposed to the reservoir. We have accounted for it by correcting α {equation (9)} as follows:

$$\frac{\alpha_{inclined}}{\alpha_{basic}} = L_{actual} \Big/ \begin{cases} L_{horizontal} & if\ h/L << 1 \\ h & if\ h/L \sim 1 \end{cases} \tag{12}$$

and treating the well as being either horizontal or vertical (whichever case is closer).

As mentioned above, the equation describing simultaneous gas-liquid flow in the reservoir (equation (2)) is difficult to solve both analytically or asymptotically. The proposed solution for this case is to use a weighted modified Joule-Thomson coefficient as follows:

$$\left(K'_{JT}\left(1 - C_{adj}/\gamma\right)\right)_{gas\_liquid} = \frac{(q)_{I,liquid}\ K'_{JT,liquid}\left(1 - C_{adj}/\gamma\right)_{liquid} + (q)_{I,gas} K'_{JT,gas}\left(1 - C_{adj}/\gamma\right)_{gas}}{(q)_I} \tag{13}$$

4.0 Rate Profiling

In this section we apply several methods for phase rate profiling in complex wells. These methods are numerically derived from equations (1a,b) in order to calculate directly the rate profiles under different boundary and flow conditions. These conditions depend on the inflow situations, the type of completion and the available downhole monitoring capabilities.

In general, equations (1a,b) can be solved numerically by an iterative process to determine the most probable phase rate values[15,16]. We can also simplify the search algorithm to direct calculations, which will then be used to demonstrate the model's abilities for fast and qualitative rate estimation. The demonstration model is an inclined, three-zone, production well containing three ICVs and one ICD (Figure 8). Input physical properties can be found in Table 4. Note that the initial analysis scenario will simulate the situation prior to the installation of the downhole equipment (it will be called the "production logging example").

4.1 Production Logging Data Analysis in a Well Prior to Completion

The number of unknown (or groups of equivalent unknown) distributions which can be estimated is limited by the number of measured profiles. E.g. to estimate one phase flow rate distribution in a well it is necessary to have one or more measured parameter distributions (e.g. the pressure profile). Two (or more) parameter profiles are required to estimate a two phase flow distribution, unless additional assumptions can be made.

In this paper we will assume that DTS, installed between the tubing and the casing walls (Figure 8), provides the temperature profile for the cases considered (this temperature profile could also have been measured by the production log in this, production logging, example). The equations presented here calculate the fluid temperature at the casing wall and in the centre of the tubing. A correction can then be applied if the available temperature profile is measured at any other radial position between them.

A more accurate estimation of the flow rate will result if more independent measurements have been made in the well. I.e. all other available measurements should be used in the analysis. We recall for the case of one phase flow (equations 1a,b; A-9

- A-12; 16) that it is sufficient to have only one measured profile (e.g. pressure or temperature) to determine the inflow rate distribution. This is only valid if the productivity index (or permeability) distribution, the reservoir pressure distribution and the correlation for the friction factor are all known. This is not always true (e.g. permeability distribution has not been estimated or reservoir pressure has changed due to depletion). Running a production log to define these profiles will supply the necessary information.

We will describe below how to estimate the rate profile if both well pressure and temperature measurements are available. This provides an independent estimation of the permeability distribution profile (and is an independent check for the case when the rate profile has been also measured). Alternatively, it can provide the rate distribution profile if the reservoir pressure profile has changed[7] due to production.

The tubing is absent prior to completion. This allows simplification of equations (1a,b) to a single equation for the well fluid temperature (similar to that previously derived for this case[17]). For the case of one phase flow it is:

$$\frac{dT_w}{dx} = \frac{2\pi R_{ci}(1-\delta)U_{wwb}(T_{wb}-T_w) + \frac{dQ}{dx}\rho C_p(T_I - T_w) + Q\rho(g\sin\theta + C_p K_{JT}\frac{dp_w}{dx})}{Q\rho C_p} \tag{14}$$

where subscript *w* stands for *well*, and *wb* for the wellbore wall (or sandface).

We rearrange equation (14) using equation (11) for the sandface temperature and the backward derivative expression as:

$$Q_w\big|_x = \left. \frac{Q_w - \frac{2\pi R_{ci}(1-\delta)U_{wwb}}{\rho C_p}\frac{\Delta x}{1+\alpha}}{1-\Delta x\left(\frac{dT_w}{dx} - \frac{g\sin\theta}{C_p} - K_{JT}\frac{dp_w}{dx}\right)\Big/\left(T_g - T_w - K_{JT}\left(1 - C_{adj}/\gamma\right)(P_e - P_w)\right)} \right|_{x-\Delta x} \tag{15}$$

We have now obtained the direct numerical equation to calculate the flow rate profile along the well length over the step Δx. Starting from the known rate value (e.g. from the heel where the (total) flow rate is known from the surface measurement), we move along the producing length, estimating the inflow profile and, via equations A-9 – A-12, the permeability (or productivity index) distribution. (Note that if one wishes to estimate the inflow profile for a well where the reservoir pressure distribution is not known then the pressure difference in the denominator of equation (15), according to equations (A-9 – A-12), should be expressed via the flow rate.)

We will illustrate this process by analysing our example well (flowing 90,000 bopd). The temperature and pressure profiles are plotted in Figures 9a,b and the estimated inflow distribution is shown in Figure 10. The resulting permeability distribution (Figure 11) successfully matches the real one.

Note that inflow temperature is not continuous. This is mainly caused by the effect of thermal interaction with adjacent layers. In general this can also be caused by a non-continuous drawdown distribution along the well (e.g. from different reservoir layers or intelligent zones), a non-uniform inflow composition, etc. The resulting flow rate distribution can be further used to estimate the friction factor correlation from the following well-known equation:

$$\frac{dp_w}{dx} = \frac{\rho f(\mathrm{Re}, \varepsilon) v^2}{R_{ci}} + \rho g \sin\theta \tag{16}$$

Note that the friction factor correlation can be different from the traditional correlations due to flow regime along inflow zones[18]. One can compare the real and estimated rate profiles for additional verification of such values as reservoir pressure, reservoir temperature if the flow rate is also measured during the production logging.

We will assume for future calculations that the well productivity index and the friction factor correlation are known.

4.2 Completed Well, One Phase Production

We will now assume the well has been completed (Figure 8) and that DTS has been installed (Figure 12). Equations (1a,b) can be rearranged as a function of only flow rates by expressing the pressure via the flow rates in equations (16, A-9 – A-12, B-2).

$$F\left(Q, Q^3, \frac{dQ}{dx}, \left(\frac{dQ}{dx}\right)^2\right) = G(k(x), T_a(x), T_g(x), T_t(x)) \tag{17}$$

We can calculate the rate profiles directly expressing equation (17) numerically on a discreet number of steps (i.e. measurement points) and defining the tubing temperature distribution (note that it can be calculated through the annular temperature using equation (1b) if is not measured). The resulting rate profile for the 70,000 bopd flowing well is plotted in Figure 13. A good match has been obtained with the actual one. Thus, we are able to track our inflow performance along the well in real-time using only temperature data.

This finding may provide sufficient justification to install DTS in many cases. The above also solves the problem of rate allocation when (unknown) changes have occurred in the zonal average pressure values. This solution has the potential to avoiding a number of regular multi-rate tests and consequent risk of failure and deferred production.

4.3 Completed Well, Two Phase Production

Knowledge of only the temperature profile is not sufficient if the well experiences two phase flow (unless we already know the particular zone which is the source of each phase). We can define rate distributions of both two phases along the well if both pressure and temperature profiles are measured (e.g. by DTS and DPS). Let us assume that combined oil-water inflow exists in the well due to water breakthrough at 3,600 bwpd at the top (60 mD) interval of the middle zone. The pressure and temperature profiles are presented in Figures 14a,b, and the change from the base case temperature profile is depicted in Figure 15. The inflow zone can be identified by the cooler temperature profile. This is mainly caused by the Joule-Thomson constant and heat capacity differences.

The direct calculation of all phase flow rates is still possible, bit is somewhat tricky:

1. We obtain the following equation for the weighted sum of the effective permeabilities by rearranging equation (1a) for this case using equations (A-9 – A-12):

$$\frac{k_o}{\mu_o}\rho_o C_{p,o}+\frac{k_{water}}{\mu_{water}}\rho_{water}C_{p,water}=\frac{\left(wC_p\right)_w\frac{dT_w}{dx}-\left(w\right)_w g\sin\theta+\left[\left(wC_pK_{JT}\right)_w\frac{dp_w}{dx}-\pi R_{ci}(1-\delta)U_{awb}(T_{wb}(x)-T_a(x))\right]}{(T_I(x)-T_a(x))\frac{4h}{Y}(P_e(x)-P_w(x))} \tag{18}$$

   Tubing, inflow and sandface temperature values in this equation are calculated using equations (1b) and (11) and the Joule-Thomson coefficient by using equation (7). Our calculations will start with a known value of the flow rate (either that at the top or a bottom of the completion) and will calculate the sum in the left hand side of equation (18).
2. Next we identify the effective permeability values. (Note that relative permeability curves should be known or assumed - in our example case we use $k_o/k_w=2$). We can now calculate the inflow of oil and water {via equations (A-9 – A-12)}.
3. We update the rate profile and move to the next spatial point and repeat the steps described in 1 and 2.

Finally we calculate the flow rate profiles for oil and water production from the annular pressures and temperatures. The results are shown in Figure 16.

4.4 Additional Sources of Information

We briefly discuss below some of the known methods of pressure and temperature interpretation which can be applied in order to increase the quality of the interpretation. Additional information is always welcome; being a source of knowledge to update, verify or increase the accuracy of estimated value of the parameters.

4.4.1 Information Obtained from Zones without Inflow

An effective method is available for absolute or relative flow rate estimation[19] along zones without inflow. Equation (1a) becomes for zones without inflow:

$$\frac{dT_a}{dx}=\frac{2\pi R_{ci}(1-\delta)U_{awb}(T_{wb}-T_a)+2\pi R_{ti}U_{at}C_{position}(T_{wb}-T_{at})+\left(w\right)_a g\sin\theta+\left[\left(wC_pK_{JT}\right)_a+h_{lat,jj'}w_{aj'}\left(\frac{\rho_{aj}}{\rho_{aj'}}\frac{dR_s}{dp}\bigg|_T\right)\right]\frac{dp_a}{dx}}{\left(wC_p\right)_a} \tag{19}$$

This does not contain the tubing temperature since it is now a dependent variable (reflected by the $C_{position}$ multiplier). The flow rate can be calculated directly from equation (19). It is equivalent to the Romero-Juarez[19] approach, but with a correction for tubing-annular thermal interaction. It can be also used to estimate the fractional flow rate if the formation heat transfer coefficient is not known.

4.4.2 Additional Information from Valves

An important source of information can be derived from the real-time measurements of pressure and temperature provided by the PDGs installed downstream the ICVs (Figure 8). Accurate calculation of the pressure drop through a valve in the case of multiphase flow is generally a difficult procedure[20]. However, a simpler description is available for liquid flow:

$$p_u-p_d=\frac{Q^2\rho}{2C_d^2A^2_{valve}}\left(1-\frac{A^2_{valve}}{A^2_{pipe}}\right) \tag{20}$$

where C_d – is the valve discharge coefficient. The temperature drop can be calculated as follows[9]:

$$T_d = T_u - C_D^2 (p_u - p_d) \frac{(wC_p K_{JT})_u}{(wC_p)_u} \tag{21}$$

and the temperature at the point where the annular fluid mixes with the tubing flow downstream the valve is given by:

$$T_{t,d} = \frac{(wC_p)_{t,u} T_{t,u} + (wC_p)_{a,u} (T_{a,u} - \Delta T_{valve})}{(wC_p)_{t,d}} \tag{22}$$

Combining some or all of equations (20-22) with the PDG's measurements allows useful information to be extracted e.g. the zonal flow rates for the case of two phase flow. Analysis of tubing pressure drop between zones {equation (16)} can also be valuable.

4.5 ICD Inflow and Annular Flow Monitoring

Annular cross-flow in ICD completions (if a packer is not installed downstream of every ICD) can result in the desired equalisation of the production or injection profiles not achieved. A significant fraction of the inflow can remain in the annulus with consequent reduction in the ICD's effectiveness. It will be shown below that it is possible to monitor and estimate this fraction that remains flowing in the annulus, using only the annular temperature profile data when single flow is present.

Note that the derivative of the annular fluid temperature changes at the position of an ICD, but that the values are continuous (Figure 17). The pressure profiles are also continuous while the tubing temperature changes stepwise (due to mixing with flow from the annulus). Thus the difference of the annular temperature derivatives {equation (1a)} for the points around the ICD position gives the following equation that connects the tubing (upstream of the ICD, Q_t), the annular rates (upstream of the ICD, Q_a) and the flow rate flowing through the ICD (Q_{at}) as:

$$\left.\frac{dT_a}{dx}\right|_u - \left.\frac{dT_a}{dx}\right|_d \approx \left(-\frac{2\pi R_{ci}(1-\delta)U_{awb}}{\rho C_p (1+\alpha)} \cdot \frac{Q_{at}}{Q_a} + \frac{Q_a}{L}\left(1 - \frac{PI_d}{PI_u} \cdot \frac{Q_a - Q_{at}}{Q_a}\right) \right) \left(T_g - T_a - \frac{K_{JT} Q_a}{L \cdot PI_u}\right) - \frac{2\pi R_{ti} C_{U_{at}} K_{JT}}{2C_d^2 A_{ICD}^2 C_p} \cdot \frac{Q_{at}^3}{Q_t} \tag{23}$$

where the coefficient $C_{U_{at}}$ represents the tubing-annular heat transfer coefficient divided by the annular flow rate (upstream of the ICD). This coefficient is almost a constant, depending mostly on the fluid properties[10]. Note that equation (23) can be further simplified if an ICD is installed in a section of uniform permeability (unlike our example, Figure 8). It also can be simplified and used if an ICD is 100% effective or 0% effective (absent) – to estimate relative change in zonal productivities.

An example calculation for the ICD inflow fraction for our completion design (Figure 8) is as follows: We assume that the total flow rate is known from surface measurements. We then calculate the inflow from the top valve {equation (20)}, the inflow rate from the ICD between the top and the middle ICVs {equation (16)} and finally the annular rate upstream of the ICD is calculated from the equation (23). In our case this indicates that only 22% of annular rate flows into the ICD. This is close to the actual value (20%). (Alternatively we could use the fact that at a small distance higher the ICD the annular temperature derivative zeroes, which gives additional dependence using equation (1a)).

The above forms the basis of an effective ICD monitoring capability. Note that in the case described above we can now adjust the ICV position in order to equalize inflow into the top zone once we know ICD inflow fraction.

5.0 Summary and Conclusions

1. This paper has emphasised the importance of a comprehensive analysis workflow that takes advantage of the complete suite of real-time, downhole data that has become available in modern completions. We have illustrated some of the tools that can be employed in the interpretation of temperature and pressure data.
2. An analysis of the scientific basis and the technical utility of available temperature modelling tools were presented. We showed that only analytical model has the potential to be developed into a real-time, well monitoring workflow.
3. The dynamic, well flow simulator has been proved to provide with independent, reference well temperature and pressure profiles.
4. The equations for calculating the temperature change around a well for the reservoir layers experiencing inflow of the reservoir fluids were derived. It was shown that it is necessary to include the interaction of the reservoir with the adjacent layers, in the calculations. Also, that the wellbore/near-wellbore thermal equilibrium changes the sandface temperature, thus decreasing heat interaction with the reservoir.
5. Several methods to directly calculate the inflow distribution into the well using different suites of measurements for complex, advanced completions were discussed:
   - **a.** Rate (and, as a result, permeability) profiling along the well length, if the temperature and pressure profiles are known.
   - **b.** Rate profiling for the completed complex well (one phase flow), based on the temperature distribution (profile) measured by DTS in the annulus.

c. Rate profiling for the completed complex well (two phase flow), based on the temperature and pressure distributions (or profiles) measured in the annulus.

d. Estimation of the fraction of annular fluid which did not enter the ICD but is flowing in the annulus. This is based on continuous temperature measurements in the annulus

e. Additionally, methods for the analysis of pressure and temperature changes across a valve have been discussed.

The presented information is a useful guide to the successful downhole data interpretation in the wells with advanced completions and, as such, is a necessary step towards comprehensive well management.

Acknowledgements

We wish to thank the sponsors of the "Added Value from Intelligent Well and Field systems Technology" Joint Industry Project at Heriot-Watt University, Edinburgh, UK, for providing financial support to one of the authors, as well as thanking SPT Group, Petroleum Experts, Schlumberger Information Systems and Weatherford (EPS) for allowing access to their software.

Nomenclature

All quantities are in SI units unless otherwise stated (Note the example cases are illustrated in field units)

A	area	R_{idc}	ideal gas constant
C_D	discharge coefficient	t	time
C_p	mass heat capacity at constant pressure	T	absolute temperature
$C_{position}$	multiplier to exclude tubing temperature (eq. 19)	U	overall heat transfer coefficient
C_{Uat}	tubing-annular heat transfer coefficient, divided by annular rate (eq. 23)	v	velocity
		V	volume
f	Moody friction factor	w	mass flow rate
g	gravity acceleration constant	w'	mass inflow rate per unit well length
h	reservoir thickness	x	spatial variable along well axis
h_{lat}	latent (transformation) enthalpy	y	spatial variable
k	permeability	Y	reservoir
K	thermal conductivity	z	z-factor (in the EOS)
K_{JT}	Joule-Thomson coefficient	α	correction term (eq 9)
K'_{JT}	modified (specifically averaged) Joule-Thomson coefficient	β	thermal expansion coefficient
		γ	denominator, used to evaluate effect of interaction with adjacent layers
L	well length (open to inflow)		
p	pressure	δ	fraction of casing area open for fluid inflow
q	volumetric flow rate	ε	roughness
Q	volumetric flow rate	θ	angle of well inclination from horizontal axis
r	radius (variable)	μ	dynamic viscosity
R	radius	ν	number of moles of a substance
R_s	solubility (in-situ)	ρ	density

Subscripts

a	annular	m	mixture
adj	adjacent (strata)	o	oil
ci	casing inner (radius)	res	reservoir
d	downstream (a valve)	t	time
e	external	ti	tubing inner (radius)
f	formation	u	upstream (a valve)
g	geothermal	w	well
I	inflow	wb	wellbore
l	liquid		

Notations

Summation of phase property(s) *f* in a volume *v* can be presented as follows: $\sum_j f_{vj} \equiv (f)_v$

Abbreviations

bopd	barrels of oil per day (downhole)	EOS	equation of state
bwpd	barrels of water per day (downhole)	ICD	inflow control device
DPS	distributed pressure sensor	ICV	interval control valve
DTS	distributed temperature sensor	PDG	permanently installed downhole gauge

References

1. Olmheim, J., *et al*: *"Autonomous Systems Improve Production"*, Journal of Petroleum Technology, May 2008, pp 66 – 73
2. Davis, B.: *"Fields of the Future Take Shape"*, Petroleum Review Journal, Dec. 2008, pp 22-24
3. Al-Khelaiwi, F.T., and Davies, D.R., *"Inflow-Control Devices"*, Journal of Petroleum Technology, Mar. 2008, pp 81-83
4. Al-Khelaiwi, F.T., *et al*: *"Advanced Wells: A Comprehensive Approach to the Selection between Passive and Active Inflow Control Completions"*, paper IPTC 12145 presented at the 2008 IPTC Conference, Kuala Lumpur, Dec. 3-5
5. Birchenko, V. *et al*: *"Impact of Reservoir Uncertainty on Selection of Advanced Completion Type"*, paper SPE 115744 presented at the 2008 SPE Annual Technical Conference and Exhibition, Denver, 21-24 Sep.
6. Al-Mutairi, F, Ph.D. Thesis, Institute of Petroleum Engineering, Heriot-Watt University, Edinburgh, U.K., 2007
7. Kulkarni, R.N. *et al*: *"Smart-Well Monitoring and Control: Snorre B Experience"*, paper SPE 109629 presented at the 2007 SPE Annual Technical Conference and Exhibition, Anaheim, Nov. 11-14
8. Govier, G., and Aziz, Kh.: "The Flow of Complex Mixtures in Pipes", 2nd edition, SPE 2008
9. Muradov, K.M., and Davies, D.R., "*Prediction of Temperature Distribution in Intelligent Wells"*, paper SPE 114772 presented at the 2008 SPE Russian Oil & Gas Technical Conference and Exhibition, Moscow, 28–30 Oct.
10. Holland, F.A., Moores, R.M., Watson, F.A. and Wilkinson, J.K.: "Heat Transfer", Heinemann Educational Books Ltd, London (1970)
11. Kim, J.Y. and Ghajar, A.J.: "*A General Heat Transfer Correlation for Non-Boiling Gas–Liquid Flow with Different Flow Patterns in Horizontal Pipes*", International Journal of Multiphase Flow 32 (2006) 447–465
12. Hasan, A.R. and Kabir C.S.: *"Heat Transfer During Two-Phase Flow in Wellbores: Part I – Formation Temperature*", paper SPE 22866 presented at the 1991 SPE Annual Technical Conference and Exhibition, Dallas, Oct. 6-9
13. Yoshioka, K. *et al*: *"Detection of Water or Gas Entries in Horizontal Wells From Temperature Profiles*", paper SPE 100209 presented at the 2006 SPE Europec/EAGE Annual Conference and Exhibition, Vienna, June 12-15
14. Zolotukhin, A.B.: "*Analytical Definition of the Overall Heat Transfer Coefficient*", paper SPE 7964 presented at the 1979 California Regional Meeting of the Society of Petroleum Engineers of AIME, Ventura, Apr. 18-20
15. Yoshioka, K. et al: *"A New Inversion Method to Interpret Flow Profiles From Distributed Temperature and Pressure Measurements in Horizontal Wells"*, paper SPE 109749 presented at the 2007 SPE Annual Technical Conference and Exhibition, Anaheim, Nov. 11-14
16. Muradov, K.M., and Davies, D.R., "*Zonal Rate Allocation in Intelligent Wells*", paper SPE 121055 presented at the 2009 SPE EUROPEC/EAGE Annual Conference and Exhibition, Amsterdam, 8–11 Jun.
17. Yoshioka, K. *et al*: *"Interpretation of Temperature and Pressure Profiles Measured in Multilateral Wells Equipped with Intelligent Completions"*, paper SPE 94097 presented at the 2005 SPE Europec/EAGE Annual Technical Conference, Madrid, June 13-16
18. Clemo, T.: *"Flow in Perforated Pipes: A Comparison of Models and Experiments"*, paper SPE 89036, 2005
19. Elshahawi, H. *et al, "Use Of Temperature Data in Gas Well Tests"*, paper SPE 56613 presented at the 1999 SPE Annual Technical Conference and Exhibition, Houston, 3–6 Oct.
20. Perkins, T.K.: *"Critical and Subcritical Flow of Multiphase Mixtures Through Chokes"*, paper SPE 20633, SPE Drilling and Completion, 1993

Appendix A: Derivation of Temperature Change across the Reservoir Containing Flowing Fluids

Equation (2) can have asymptotic solutions because certain conditions (conditional equations (4-5)) are normally valid:

$$\sum_j \vec{v}_j \left[\rho_j C_{p,j} \vec{\nabla} T_f + (1-\beta_j T_f)\vec{\nabla} p_j\right] - \vec{\nabla}(\overline{\overline{K_f}}\vec{\nabla} T_f) + 2U_{adj}(T_f - T_{f,geothermal})/h = 0 \quad \text{(A-1)}$$

The boundary and initial conditions can be described mathematically as[13]:

$$T_f\Big|_{external\ boundary} = T_e = T_g \quad \textit{(external temperature does not vary with time)} \quad \text{(A-2)}$$

$$K_f \left.\frac{dT_f}{dr}\right|_{r=R_{wb}} = \frac{R_{ci}}{R_{wb}} U_{awb}(T_f\Big|_{r=Rwb} - T_a) \quad \textit{(heat transfer in the well is at steady state)} \quad \text{(A-3)}$$

for both the vertical and horizontal well cases. The asymptotic solution of equation (A-1) is (Equation 11):

$$T_{wb} \approx T_e - \frac{K'_{JT}(1 - C_{adj}/\gamma)(P_e - P_{wb}) - \alpha(T_a - T_e)}{1+\alpha} \quad \text{(A-4)}$$

where the modified Joule-Thomson coefficient K'_{JT}, the correction multiplier γ and the contributing reservoir area in C_{adj} (equation (8)) are case specific. The correction term α is common and described by equation (9). Schematic diagrams for the horizontal and vertical well cases are presented in Figure 5 and Figure 6.

Solution of equation (A-1) requires definition of functions for the fluid pressure, density and velocity. The steady-state pressure and velocity distribution is obtained from Darcy's equation for the radial:

$$v_j(r) = \frac{q_j}{2\pi rh} = -\frac{k_j}{\mu_j}\frac{dp_j}{dr} \tag{A-5}$$

and the linear flow cases:

$$v_j(y) = \frac{q_j}{2Lh} = -\frac{k_j}{\mu_j}\frac{dp_j}{dy} \tag{A-6}$$

The gas density is the reciprocal function of the volumetric flow rate at steady-state. It is defined by the Equation of State. We used the average density for liquids and the classical EOS with z-factor for real gases:

$$pV = z\nu R_{idc}T \tag{A-7}$$

The z-factor and its first-derivative can be taken as constants since they show little variation under reservoir conditions. If we assume the reservoir to be adiabatic and thermally no-conducting (see section 3.2) we can calculate the value of the case specific, modified Joule-Thomson coefficient:

$$K'_{JT} = -\frac{T_e - T_{wb}}{P_e - P_{wb}} = -\frac{\int_{R_{wb}}^{\frac{Y}{2}orR_e}\vec{\nabla}T dV}{P_e - P_{wb}} \overset{from\ Eq\,(A\text{–}1)}{=} -\int_{R_{wb}}^{\frac{Y}{2}orR_e}\frac{\sum_j \vec{v}_j(1-\beta_j T_f)\vec{\nabla}p_j dV}{\sum_j \vec{v}_j\rho_j C_{p,j\,j}} \tag{A-8}$$

Further, we solve the general equation (A-1) (with zero formation thermal conductivity) to account for the thermal interaction of the reservoir with adjacent layers. The results are presented in Table 3.

The main emphasis in the above downhole data analysis is oriented towards the problem of estimating flow rates when pressure data is not available. However, the results in equation (A-2) and Table 3 are dependent on the pressure values. Hence we present below some well-known, inflow performance relationship dependencies (derived directly from equations A-5, A-6 and A-7), which can be used with rate data as a substitute for the pressure data:

Case 1. Liquid producing horizontal well:

$$q_j = \frac{4Lhk_j}{\mu_j Y}(P_e - P_{wb}) \tag{A-9}$$

Case 2. Gas producing horizontal well:

$$q_j = \frac{4Lhk_j}{\mu_j Y}\frac{(P_e^2 - P_{wb}^2)}{2P_{wb}} \tag{A-10}$$

Case 3. Liquid producing vertical well:

$$q_j = \frac{2\pi hk_j}{\mu_j \ln(\frac{R_e}{R_{wb}})}(P_e - P_{wb}) \tag{A-11}$$

Case 4. Gas producing vertical well:

$$q_j = \frac{2\pi hk_j}{\mu_j \ln(\frac{R_e}{R_{wb}})}\frac{(P_e^2 - P_{wb}^2)}{2P_{wb}} \tag{A-12}$$

Tables

	True (base case)	Predicted with		
		Steady state well simulators	Thermal reservoir and well simulator	Dynamic well simulator
Q_{tubing}, stbopd	500	400 ± 100	700 ± 150	500 ± 100
$Q_{annular}$, stbod	500	11000 ± 2000	350 ± 100	500 ± 100

Table 1: Comparison of true flow rates with predicted values obtained by matching temperature data using other simulation models

Model \ Ability	Heat exchange between pipes	Heat transfer coefficient calculation	Predict Flow rates from Temperature data
Steady-state well flow simulators	No	Yes	NR*
Reservoir/well flow simulator	Yes	Yes	NR*
Dynamic well flow simulator	Yes	Yes	Low
Analytical model	Yes	Yes	High

Table 2: The key effects in I-wells and the ability of software and theoretical models to account for them (NR* = Not Recommended)

Case \ Coefficient (in equation (11))	Modified Joule-Thomson Coefficient K'_{JT}	Adjacent layers thermal interaction correction multiplier, γ	$A_{res,I}$ in C_{adj} (see Eq. (8) and Figures 5, 6)
Horizontal well, liquid flow	$-\frac{k_o}{\mu_o q_o}\frac{1}{(wC_p)_I}\left(\frac{q^2\mu}{k}\right)_I\left[1-T_e\left(\frac{\beta q^2\mu}{k}\right)_I\Big/\left(\frac{q^2\mu}{k}\right)_I\right]$	1	LY
Horizontal well: gas flow	$\left(\frac{T}{z}\left(\frac{dz}{dT}\right)_P\right)_e\left(\frac{P}{C_p\rho}\right)_{wb}\frac{\ln(P_e/P_{wb})}{P_e-P_{wb}}$	$\ln(P_e/P_{wb})$	LY
Vertical well: liquid flow	As for horizontal well	$\ln(R_e/R_{wb})$	πR_e^2
Vertical well: gas flow	As for horizontal well	$\frac{\exp\left(\frac{2P_e^2\ln(Re/Rwb)}{P_e^2-P_{wb}^2}\right)}{4}$	πR_e^2

Table 3: Coefficients used to calculate temperature changes in the reservoir {Equation (11)}

property / medium	Cp	K	μ	ρ	β
	Btu/lbm/R	Btu/hr/ft/R	cP	lbm/ft3	1/R
oil	0.64	0.09	0.2	36	0.0009
water	0.95	0.34	0.34	64	0.0001
gas	0.7	0.03	0.03	16	0.0027
cement	0.6	1	-	100	-
formation	0.6	1.75	-	135	-
packer (steel)	0.1	10	-	490	-

Table 4: Values of physical properties at in-situ conditions

Figures

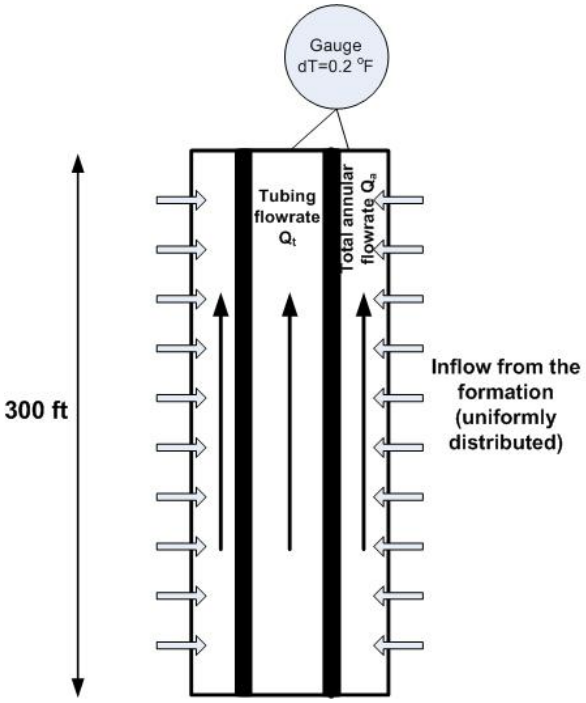

Figure 1: Schematic view of the single segment used for comparison of the temperature modeling tools

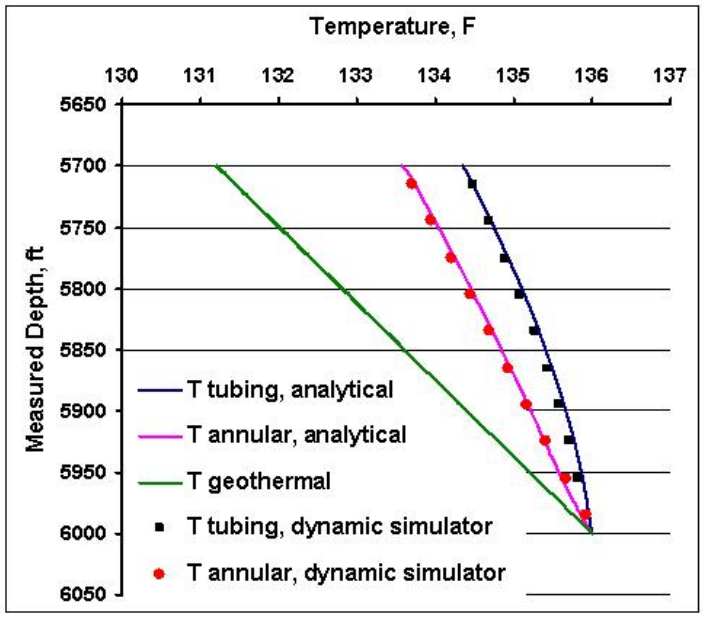

Figure 2: Temperature profiles comparison: analytical and dynamic well flow simulator results

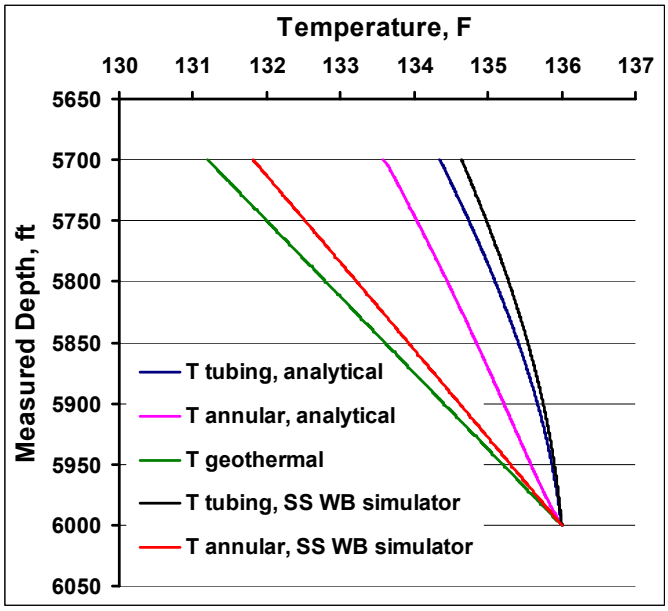

Figure 3: Temperature profiles compared: analytical and steady-state well flow simulators results

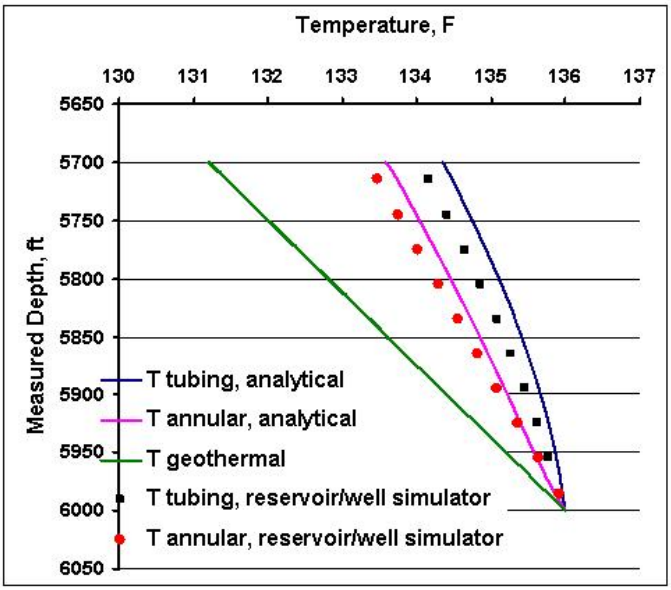

Figure 4: Temperature profiles compared: analytical and reservoir simulation results

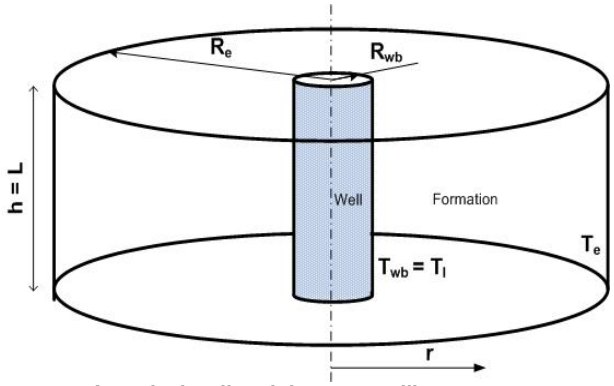

Figure 5: A vertical well and the near-wellbore zone

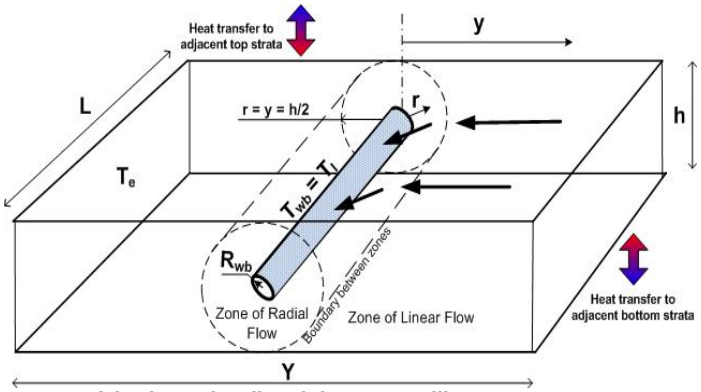

Figure 6: A horizontal well and the near-wellbore zone

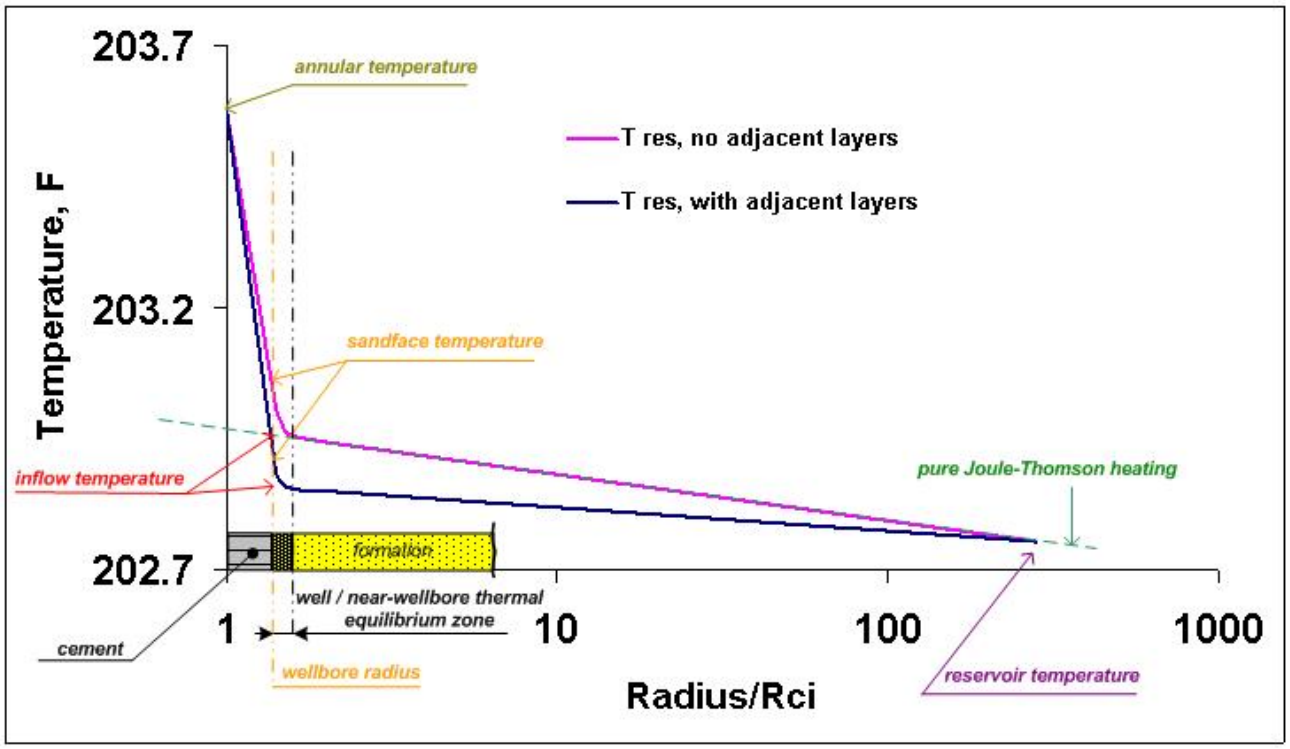

Figure 7: Example temperature distribution in the reservoir around a vertical well

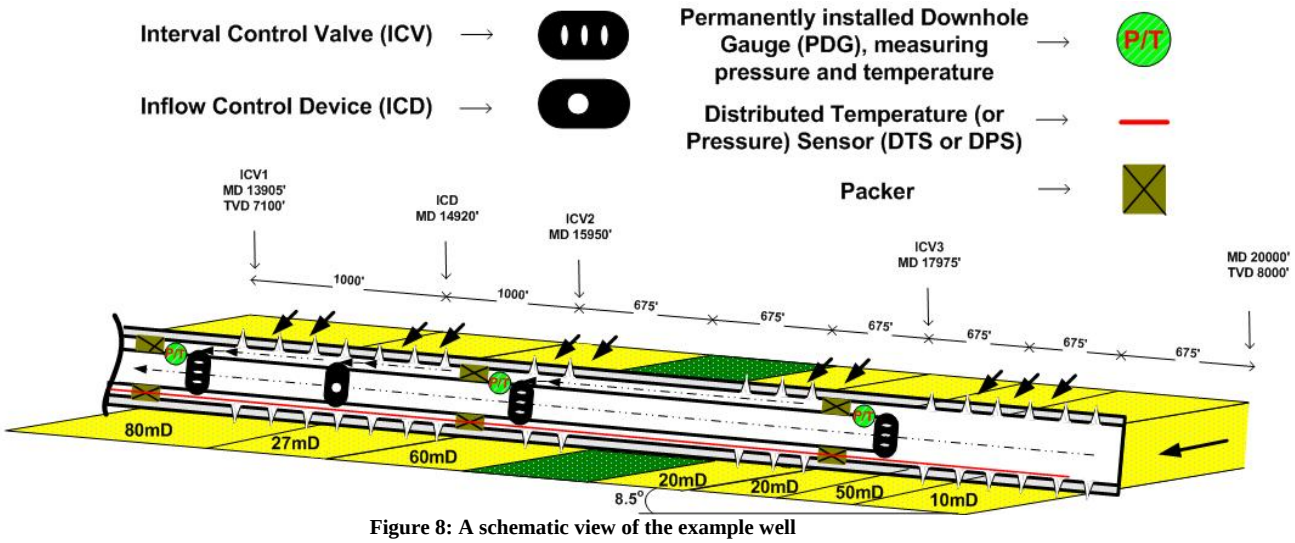

Figure 8: A schematic view of the example well

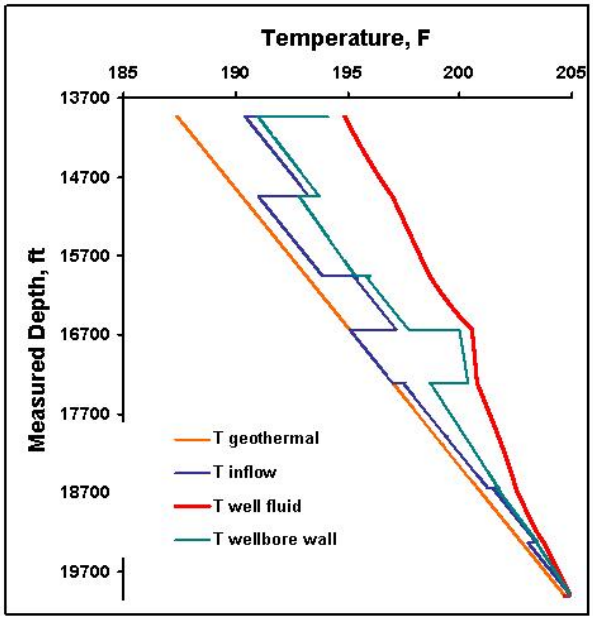

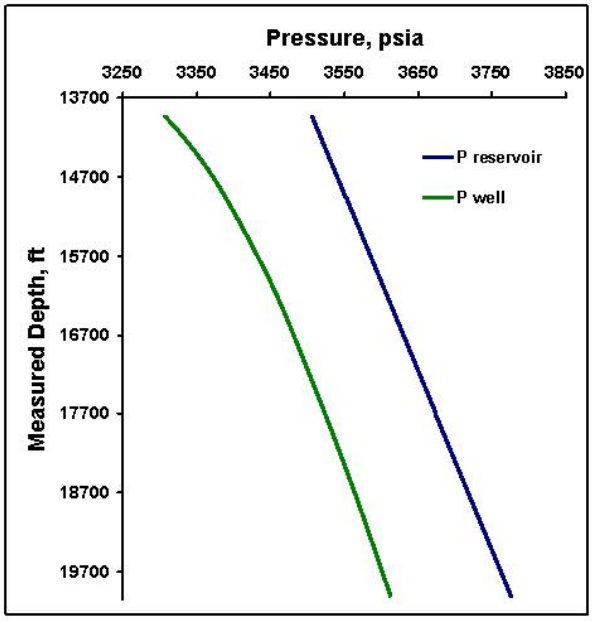

Figures 9a,b: Temperature and pressure distribution: Production logging case

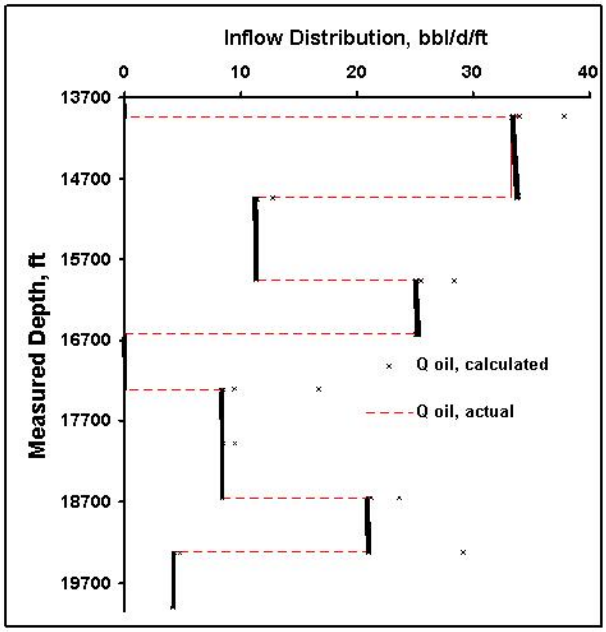

Figure 10: Inflow distributions: Production logging case

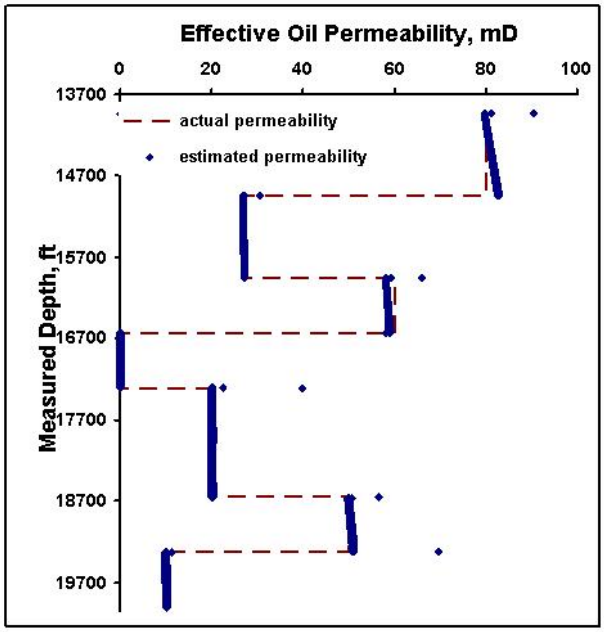

Figure 11: Permeability distribution: Production logging case

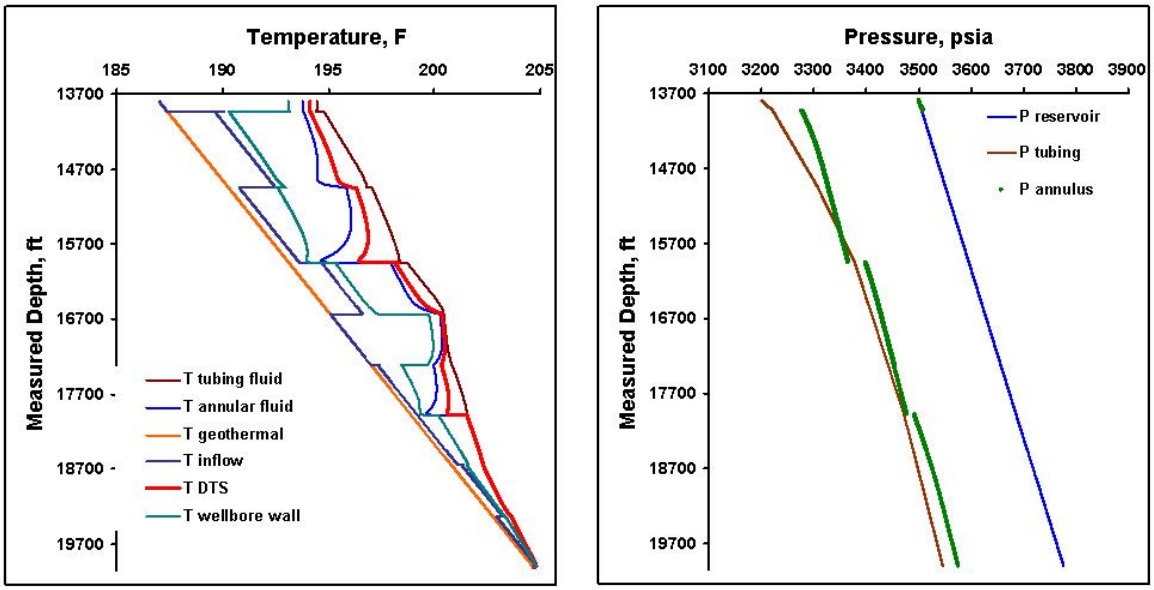

Figure 12: Temperature and pressure distribution: One phase flow in a completed well

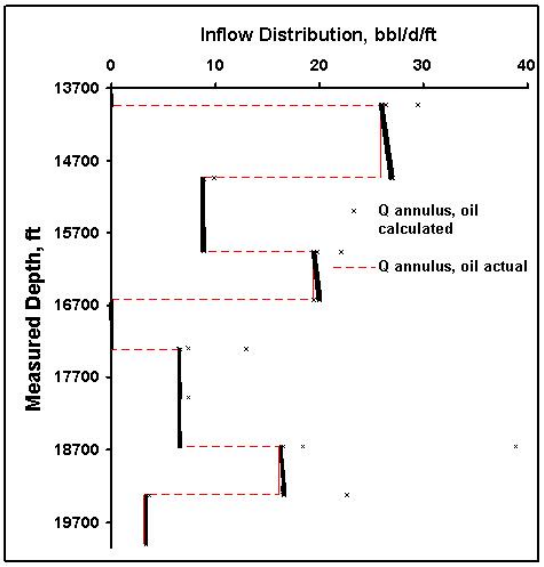

Figure 13: Inflow distribution: One phase flow in a completed well

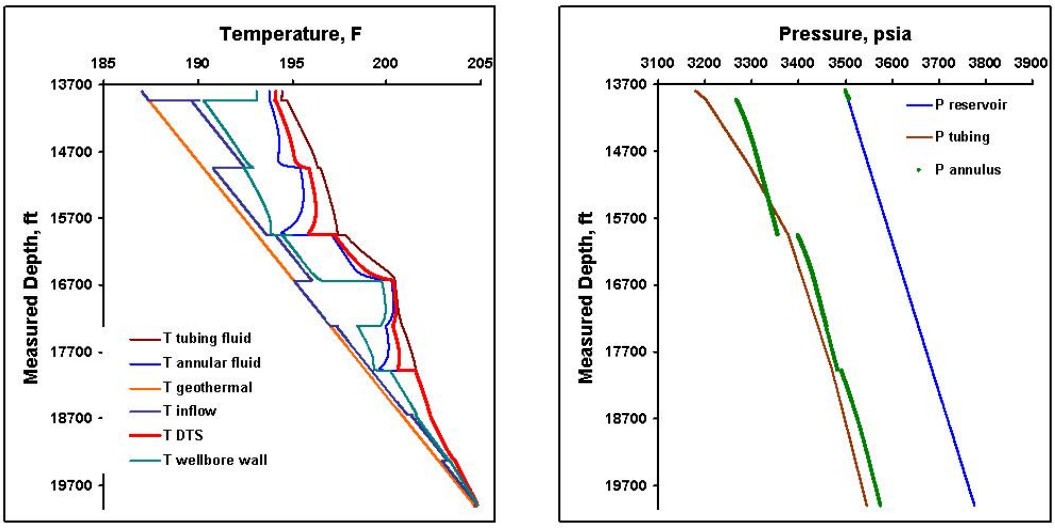

Figures 14 a,b: Temperature and pressure distribution: Two phase flow in a completed well

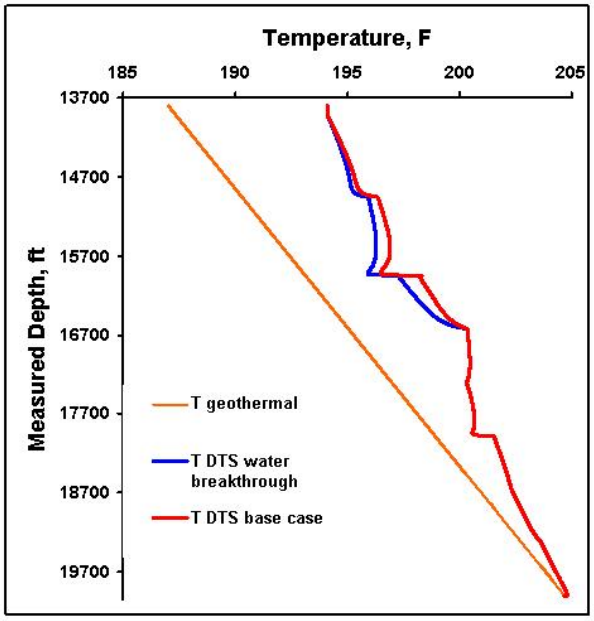

Figure 15: Temperature profiles compared: One and two phase flow in a completed well

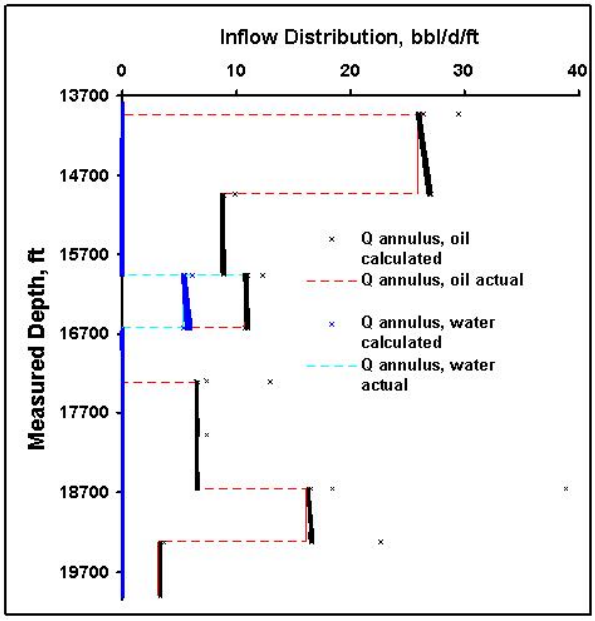

Figure 16: Inflow distribution compared: Two phase flow in a completed well

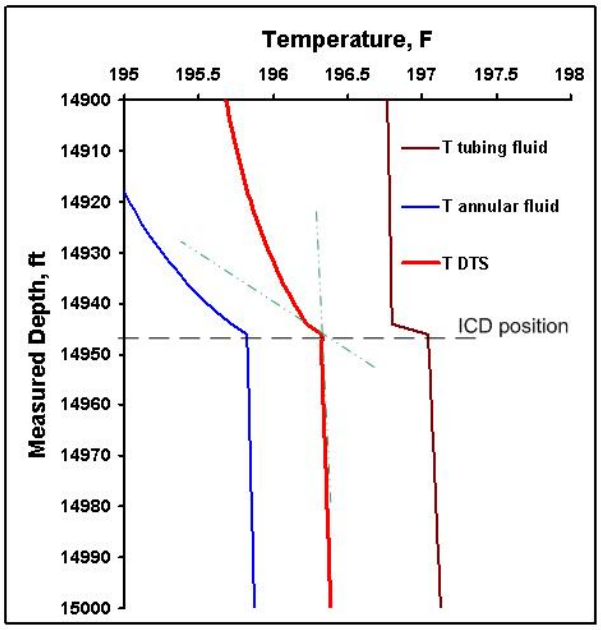

Figure 17: Calculation of the fluid fraction inflowing into the ICD